Proceedings of the 17th World Congress
The International Federation of Automatic Control
Seoul, Korea, July 6-11, 2008

Modeling and Parameter Estimation of Endothelial Cells ⋆

Er-Wei Bai * **Sunaina Fotedar** ** **Alan Moy** ***

* *Dept. of Electrical and Computer Engineering, University of Iowa, Iow a City, IA 52242 USA (e-mail: er-wei-bai@uiowa.edu).*
** *Kennedy Krieger Institute, John Hopkins University*
*** *Cellular Engineering Technologies, Inc.*

Abstract: A nonlinear identification approach for modeling endothelial cells is mathematically derived and experimentally tested under the realistic alternating current voltage and a square-like shape assumptions. Results demonstrate the applicability and effectiveness of the approach. The derived model is an important step in understanding a cell system and in developing controlling and treating certain disorders by new drugs.

1. INTRODUCTION

The aim of this work is to develop and test an identification approach to model a cell system, in particular endothelial cells. Such a model is essential in understanding a cell system and in developing controlling and treating certain disorders by new drugs.

Endothelial cells play a crucial role in maintaining vascular homeostasis [14]. They perform a large array of physiological functions that are influenced by their cellular homogeneity in the different vascular beds [2]. They are vital for the proper functioning of blood vessels wherein these endothelial cells line blood vessels and help regulate blood flow, inhibit smooth muscle cell overgrowth, and resist thrombosis. The endothelium lining the inner wall of blood vessel is a complex physiological system playing a crucial role in modulating vessel tone and remodeling the blood flow and barrier function [2].

The functions of various kinds of endothelial cells have been extensively studied by means of *in vitro* cultures. *In vivo* models represent an essential tool for the study of specific cellular and molecular mechanisms involved in physiology and pathophysiology [14]. Studies have shown that the endothelial adherent junctions regulate the transendothelial flux of liquid and plasma proteins [5]. The structural and functional integrity of the endothelium is an essential requirement for its semiselective barrier properties between the blood stream and the underlying tissues. The maintenance of a continuous endothelial cell monolayer of tightly opposed cells is also central for preventing the vessel wall from platelet deposition and thrombus formation. Vascular endothelial cell monolayer functions as a barrier between the blood and interstitial compartments. A decrease in the barrier properties of vascular endothelium leads to tissue edema [16]. Morphological studies *in vitro* and *in vivo* have shown the presence of tight junctions and gap junctions between adjacent endothelial cells [13]. Cell-cell adhesion structures have also been extensively studied and specific molecules of both the calcium dependent and independent cell adhesion mechanisms have been identified [8]. In spite of recognizing the importance and the molecular morphological organization of cell-cell junctions in the maintenance of endothelial functional properties, however, little is known how these adhesion sites are regulated. For technical reasons, the electrophysiological investigation of these cells *in situ* has not been possible so far and therefore a number of questions concerning their basic function remain open. In addition, though we are aware that the endothelial cells form a tight syncytium, very little is known about the degree of electrical coupling between them *in situ* and *in vivo* conditions. The cytoskeleton of endothelial cells is an integrated network of filaments and adhesion proteins in which forces at cell-cell regions are mechanically coupled to cell-matrix regions [8, 9, 10]. These cell-cell and cell-matrix sites are mechanically coupled by an intervening series of filamentous cytoskeleton that can transfer local mechanical forces to distal sites. The cell-cell and cell matrix adhesive sites provide a resistive barrier for the passage of macromolecules across a monolayer. Thus, having models that can break down barrier function into separate indices of cell-cell and cell-matrix adhesion would represent an important milestone. For instance, inflammatory disorders, angiogenesis, oncogenesis, cell toxicity, and wound repair depend on alterations in endothelial cell-cell and cell-matrix adhesion. One application of the model is to derive quantitative measurements under different drug stimulus conditions. Numerical modeling seems to be the most effective way to provide information on cell-cell and cell-matrix adhesion and membrane capacitance and is a critical step in understanding disease processes and in developing new drugs treating these disorders [6, 8].

It is clear that modeling and identification of a complex cell system is unlike a typical engineering modeling problem [7, 11, 15] and imposes a very challenging problem to the identification community. On the other hand, developing a mathematical model to evaluate complex biological systems can provide insights and reduce the cost and time of biological research. Giaever was the first [3, 4] to introduce a model that characterizes transcellular impedance across a cell-covered electrode into indices of cell-cell and cell-

⋆ This work was supported in part by by NSF ECS-0555394 and NIH/NIBIB EB004287.

matrix adhesion. He characterized transcellular impedance of a cell-covered electrode as an electrical circuit consisting of a capacitor and resistor in series. The model characterizes transcellular impedance into three unknown solution parameters in confluent cultured cells, the impedance due to cell-cell adhesion, the impedance due to cell-matrix adhesion and the membrane capacitance due to transcellular electrical conduction. These solutions can be resolved by measuring the experimental impedance at multiple current frequencies. A problem to his approach is the lack of details on how the model was obtained. No complete mathematical derivation of the model has ever been published. Therefore, it is hard if possible to check the validity of the approach or make modification of the model. Also, a resistive component of the cell membrane was ignored in [3, 4]. To this end, we have develop a model [1] which assumes direct current (DC) voltage though the model was tested in the alternating current (AC) voltage cases and demonstrated good fits. Both Giaever and our early works [1, 3, 4] assumed a disk-shaped cell shown in Figure 1a. This was a critical assumption that was overly simplified but was necessary to be able to derive a mathematical model. In reality, an endothelial cell is not disk shaped but is more of a square shape [8], see Figure 1b, without empty space between adjacent cells. In [1], it was shown that a simple R-C series model based on a disk shape structure was not good enough. Therefore, there is a need to develop a model based on a more realistic cell shape. The difference between a disk-like shape and a square-like shape could be significant because they introduce different boundary conditions for modeling.

The contribution of the paper is to develop and test a model for a square-like shape cell that takes care explicitly of sinusoidal AC voltage input. To the best of our knowledge, the square-like shape cell has never been considered in the literature.

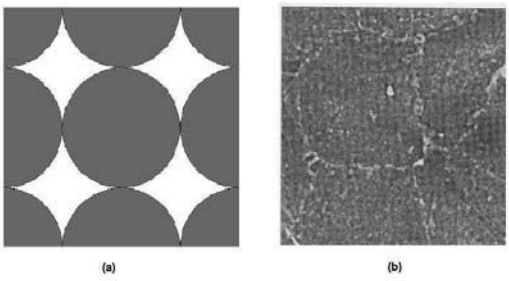

Fig. 1. (a) Assumed disk cell shape. (b) Observed cell shape.

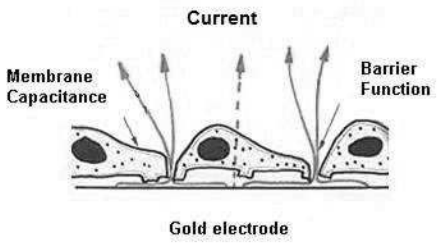

Fig. 2. Illustration of the cell system.

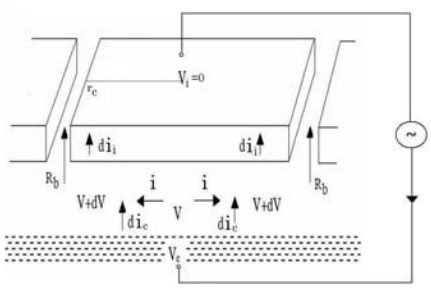

Fig. 3. Model schematics.

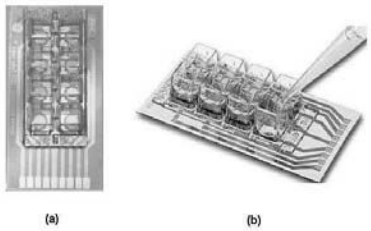

Fig. 4. (a) Gold electrodes. (b) Cells are grown in wells.

2. MODEL AND IDENTIFICATION

2.1 Model set-up

To derive a model for a square-like shape cell system, consider the cell system as in Figure 2. An experiment shown in Figure 3 was designed [1, 8], where cells are cultured on small gold electrodes shown in Figure 4. The total impedance $Z_c(\omega)$, as a function of the input frequency ω, is calculated as the ratio of the applied voltage and the measured current. The area of an endothelial cell is in the range of $400 \cdot 10^{-9} m^2$. At this level, three primary paths of current can be found flowing across a confluent monolayer. Each path of current is affected by small spatial changes in the cellular shape, which dynamically modifies transendothelial impedance. The first path of current flow $i(t, r)$ lies between the ventral surface of the monolayer and the surface of the naked electrode, where r is the distance from the cell center. The current is determined by the parameter α, which is expressed in units of $\sqrt{\Omega}cm$. The α term is defined by the expression, $\alpha = r_c\sqrt{\rho/h}$, which is dependent on the average separation distance $h(nm)$ between the ventral membrane surface and the substratum, the solution resistivity $\rho(\Omega cm)$ of the culture medium, and the cell side length $2r_c(cm)$. The path of current flow between the adjacent edges of the cells within the monolayer is labeled with the impedance R_b expressed in units of $\Omega \cdot cm$. The final path of current has a capacitive component and relates to transcellular-cellular current flow through a ventral and dorsal plasma membrane. The transcellular-cellular current $i_i(t, r)$ is dominated by the membrane capacitance parameter $C_m(F/cm^2)$ along with a trans-membrane resistance $R_m(\Omega cm^2)$. These four parameters C_m, R_m, α and R_b represent a cell's properties. The values of these parameters vary depending on the biological behavior of the cell which can be regulated by intracellular and extracellular factors. The purpose of

identification/modeling is to estimate the values of these parameters under different physiological and pathological conditions.

2.2 Mathematical derivation

Now, let $v_c(t) = Csin(\omega t)$ be the voltage present at the surface of the electrode where C is a constant and ω is the input frequency. Let $v(t,r)$ be the voltage present in the space between cells ventral surface and the electrode surface at location r from the cell center, and $v_i(t,r)$ the voltage along the apical surface of the cell. For an endothelial cell, the height is so thin so $v_i(t,r)$ can be considered zero for all t and r. Current $di_c(t,r)$ flows vertically from the electrode surface and a change in current $di_c(t,r)$ occurs when a part of current $di_i(t,r)$ penetrates the cell membrane. A change in voltage, $dv(t,r)$, takes place as current $di(t,r)$ spreads horizontally in the space between cells ventral surface and the electrode surface. We assume that voltage potential $v(t,r)$ remains the same on the edge of any square centered at the origin of a cell. By applying Ohm and Kirchoff laws, it follows that

$$-dv(t,r) = \frac{1}{8hr}\rho i(t,r)dr$$

$$v_c(t) - v(t,r) = \frac{1}{8rdrc_n}\int_{-\infty}^{t} di_c(t,r)dt + \frac{R_n}{8rdr}di_c(t,r)$$

$$v(t,r) - v_i(t,r) = \frac{1}{8rdrc_m}\int_{-\infty}^{t} di_i(t,r)dt + \frac{R_m}{8rdr}di_i(t,r)$$

$$di(t,r) = di_c(t,r) - di_i(t,r) \qquad (1)$$

where the differentiation is with respect to the distance r and the voltage $v_c(t) = Csin(\omega t)$, $\omega > 0$ is a single frequency sinusoidal wave uniformly on the electrode. $C_n(F/cm^2)$ and $R_n(\Omega cm^2)$ are the capacitance and resistance of the naked electrode.

The first equation describes the horizontal drop in voltage in the ventral space below the cell as it spreads radically from the center of the cell towards its outer edges. This horizontal voltage drop is governed by ρ and h, which have been previously defined. The second equation describes the vertical change in voltage from the electrode surface into the medium below the ventral surface of the cell. The third equation describes the change in voltage from the ventral to apical surfaces of the cell membrane. The final equation is the Kirchoff's current law. What we are interested is the steady state response of the cell system which is modeled by linear resistors and capacitors. Thus, Fourier transform applies and this leads to

$$-dV(\omega,r) = \frac{1}{8hr}\rho I(\omega,r)dr$$

$$V_c(\omega) - V(\omega,r) = \frac{1}{8rc_nj\omega}\frac{dI_c(\omega,r)}{dr} + \frac{R_n}{8r}\frac{dI_c(\omega,r)}{dr}$$

$$= \frac{1}{8r}Z_n(\omega)\frac{dI_c(\omega,r)}{dr}$$

$$V(\omega,r) = \frac{1}{8r}Z_m(\omega)\frac{dI_i(\omega,r)}{dr}$$

$$dI(\omega,r) = dI_c(\omega,r) - dI_i(\omega,r)$$

where $V(\omega,r)$, $I(\omega,r)$, $I_c(\omega,r)$, $I_i(\omega,r)$ and $V_c(\omega)$ are the Fourier transforms of $v(t,r)$, $i(t,r)$, $i_c(t,r)$, $i_i(t,r)$ and $v_c(t)$ respectively. With

$$Z_n(\omega) = \frac{1}{j\omega c_n} + R_n, \quad Z_m(\omega) = \frac{1}{j\omega c_m} + R_m$$

these four equations lead to

$$-\frac{d^2V(\omega,r)}{dr^2} = \frac{\rho}{8hr}\frac{dI(\omega,r)}{dr} - \frac{\rho}{8h}I(\omega,r)\frac{1}{r^2}$$

$$= \frac{\rho}{8hr}(\frac{dI_c(\omega,r)}{dr} - \frac{dI_i(\omega,r)}{dr}) - \frac{\rho}{8hr}I(\omega,r)\frac{1}{r}$$

$$= -\underbrace{\frac{\rho}{h}[\frac{1}{Z_n(\omega)} + \frac{1}{Z_m(\omega)}]}_{\gamma^2(\omega)}V(\omega,r) + \underbrace{\frac{\rho}{h}\frac{V_c(\omega)}{Z_n(\omega)}}_{\beta(\omega)} + \frac{1}{r}\frac{dV(\omega,r)}{dr}$$

and

$$\frac{d^2V(\omega,r)}{dr^2} + \frac{1}{r}\frac{dV(\omega,r)}{dr} - \gamma^2(\omega)V(\omega,r) + \beta(\omega) = 0$$

This is the Bessel equation and its solution can be easily derived

$$V(\omega,r) = AI_0(\gamma(\omega)r) + BK_0(\gamma(\omega)r)) + \frac{\beta(\omega)}{\gamma^2(\omega)}$$

where $I_0(\gamma(\omega)r)$ and $K_0(\gamma(\omega)r)$ are the modified Bessel functions of the first and second kinds, respectively. Since $|K_0(\gamma(\omega)r)| \to \infty$ as $r \to 0$, the coefficient $B = 0$ and this implies

$$V(\omega,r) = AI_0(\gamma(\omega)r) + \frac{\beta(\omega)}{\gamma^2(\omega)}$$

By the assumption that a cell is square shaped and the side length of a cell is $2r_c$, it follows that

$$\frac{\beta(\omega)}{\gamma^2(\omega)} = \frac{Z_m(\omega)}{Z_n(\omega) + Z_m(\omega)}V_c(\omega)$$

or

$$V(\omega,r) = AI_0(\gamma(\omega)r) + \frac{Z_m(\omega)}{Z_n(\omega) + Z_m(\omega)}V_c(\omega)$$

for some constant A. To determine the constant A, we have to calculate the total current $I_{it}(\omega)$ that penetrates the cell membrane and and the total current $I_{ct}(\omega)$ that flows vertically from the electrode surface. To this end, we have

$$I_{it}(\omega) = \int_0^{r_c}\frac{8r}{Z_m(\omega)}\frac{dI_i(\omega,r)}{dr}dr = \int_0^{r_c}\frac{8r}{Z_m(\omega)}V(\omega,r)dr$$

$$= \frac{8}{Z_m(\omega)}\int_0^{r_c}[ArI_0(\gamma(\omega)r) + \frac{Z_m(\omega)}{Z_n(\omega) + Z_m(\omega)}V_c(\omega)r]dr$$

$$= \frac{8r_cA}{Z_m(\omega)\gamma(\omega)}I_1(\gamma(\omega)r_c) + \frac{4r_c^2V_c(\omega)}{Z_n(\omega) + Z_m(\omega)}$$

Similarly,

$$I_{ct}(\omega) = \int_0^{r_c}\frac{dI_c(\omega,r)}{dr}dr = \int_0^{r_c}\frac{8r}{Z_n(\omega)}(V_c(\omega) - V(\omega,r))dr$$

$$= \frac{4r_c^2}{Z_n(\omega)}V_c(\omega) - \frac{8}{Z_n(\omega)}\int_0^{r_c}[ArI_0(\gamma(\omega)r) + r\frac{Z_m(\omega)}{Z_n(\omega) + Z_m(\omega)}V_c(\omega)]dr$$

$$= -\frac{8r_cA}{Z_n(\omega)\gamma(\omega)}I_1(\gamma(\omega r_c) + \frac{4r_c^2}{Z_n(\omega) + Z_m(\omega)}V_c(\omega)$$

where $I_1(\gamma(\omega)r)$ is the modified Bessel function of the first kind of order 1. Therefore, the total current $I(\omega, r)$ at $r = r_c$ is obtained

$$I(\omega, r_c) = I_{ct}(\omega) - I_{it}(\omega)$$
$$= -\frac{8r_cA}{\gamma(\omega)} I_1(\gamma(\omega)r_c)(\frac{1}{Z_n(\omega)} + \frac{1}{Z_m(\omega)})$$

Now note

$$V(\omega, r_c) = AI_0(\gamma(\omega)r_c) + \frac{Z_m(\omega)}{Z_n(\omega) + Z_m(\omega)} V_c(\omega)$$

Again by the assumption that a cell is square shaped, we have at $r = r_c$,

$$V(\omega, r_c) = I(\omega, r_c)\frac{R_b}{8r_c} = -\frac{A}{\gamma(\omega)} I_1(\gamma(\omega)r_c)(\frac{1}{Z_n(\omega)} + \frac{1}{Z_m(\omega)})R_b$$

Thus,

$$A = \frac{\frac{-Z_m(\omega)}{Z_n(\omega)+Z_m(\omega)} V_c(\omega)}{I_0(\gamma(\omega)r_c) + \frac{R_b}{\gamma(\omega)} I_1(\gamma(\omega)r_c)(\frac{1}{Z_n(\omega)} + \frac{1}{Z_m(\omega)})}$$

This solves A. To find the equivalent total impedance $Z_c(\omega)$, we note

$$\frac{Z_c(\omega)}{4r_c^2} = \frac{V_c(\omega)}{I_{ct}(\omega)}$$
$$\Longrightarrow \frac{1}{Z_c(\omega)} = \frac{1}{Z_n(\omega)}\{\frac{Z_n(\omega)}{Z_n(\omega) + Z_m(\omega)}$$
$$+ \frac{\frac{Z_m(\omega)}{Z_n(\omega)+Z_m(\omega)}}{\frac{1}{2}\gamma(\omega)r_c\frac{I_0(\gamma(\omega)r_c)}{I_1(\gamma(\omega)r_c)} + \frac{r_c}{2}R_b(\frac{1}{Z_n(\omega)} + \frac{1}{Z_m(\omega)})}\}$$

Finally, from $\gamma(\omega)r_c = \alpha\sqrt{\frac{1}{Z_n(\omega)} + \frac{1}{Z_m(\omega)}}$, we have

$$\frac{1}{Z_c(\omega)} = \frac{1}{Z_n(\omega)}\{\frac{Z_n(\omega)}{Z_n(\omega) + Z_m(\omega)} + \qquad (2)$$

$$\frac{\frac{Z_m(\omega)}{Z_n(\omega)+Z_m(\omega)}}{\frac{\alpha}{2}\sqrt{\frac{1}{Z_n(\omega)} + \frac{1}{Z_m(\omega)}}\frac{I_0(\alpha\sqrt{\frac{1}{Z_n(\omega)} + \frac{1}{Z_m(\omega)}})}{I_1(\alpha\sqrt{\frac{1}{Z_n(\omega)} + \frac{1}{Z_m(\omega)}})} + \frac{r_c}{2}R_b(\frac{1}{Z_n(\omega)} + \frac{1}{Z_m(\omega)})}\}$$

This is the model by assuming a square shaped cell. The model contains a number of parameters, $Z_c(\omega)$, $Z_n(\omega)$, $Z_m(\omega) = R_m + \frac{1}{j\omega c_m}$, R_b, α and r_c. Among them, $Z_c(\omega)$ is the total impedance and $Z_n(\omega)$ the impedance without cell covering. Both $Z_c(\omega_i)$ and $Z_n(\omega_i)$ are measured experimentally at each input frequency ω_i. The "radius" r_c also comes into the model, a unique property of a square shaped cell model. Four unknown parameters are α, R_b, R_m and c_m that describe the cell's properties.

2.3 Identification algorithm

The model (2) involves four unknown parameters α, R_b, R_m and c_m that represent a cell system properties and are what we try to estimate from experimental data. To estimate these unknown parameters, inputs have to be applied repeatedly at different frequencies and the corresponding $Z_c(\omega_i)$ for the cell covered electrode and $Z_n(\omega_i)$ for the naked cell electrode, $i = 1, 2, ..., N$, are measured. Now suppose $\widehat{\alpha}$, $\widehat{R}_b$, $\widehat{R}_m$ and $\widehat{c}_m$ are some estimates of α, R_b, R_m and c_m respectively, an estimate $\widehat{Z}_m(\omega)$ of $Z_m(\omega)$ can be defined as $\widehat{Z}_m(\omega) = \widehat{R}_m + \frac{1}{j\omega\widehat{c}_m}$. Similarly an estimate $\widehat{Z}_c(\omega)$ of $Z_c(\omega)$ based on $\widehat{\alpha}$, $\widehat{R}_b$, $\widehat{R}_m$ and $\widehat{c}_m$ is defined by (2) by replacing $Z_m(\omega)$, α, R_b, R_m and c_m by $\widehat{Z}_m(\omega)$, $\widehat{\alpha}$, $\widehat{R}_b$, $\widehat{R}_m$ and $\widehat{c}_m$ respectively.

The optimal estimates α^*, R_b^*, R_m^* and c_m^* are defined as those that minimize the following cost function

$$(\alpha^*, R_b^*, R_m^*, c_m^*) = arg \min_{\widehat{\alpha}, \widehat{R}_b, \widehat{R}_m, \widehat{c}_m} \sum_{i=1}^{N} |\frac{Z_c(\omega_i)}{Z_n(\omega_i)} - \frac{\widehat{Z}_c(\omega_i)}{Z_n(\omega_i)}|^2 \qquad (3)$$

where N is the number of frequencies at each experiment. The idea is that the difference between the predicted $\widehat{Z}_c(\omega)/Z_n(\omega)$ and the measured $Z_c(\omega)/Z_n(\omega)$ is minimized. This is a nonlinear optimization problem and the well known Levenberg-Marquardt nonlinear least squares algorithm [12] was used in our experiments and calculations.

3. EXPERIMENTAL RESULTS

3.1 Material and equipments

Fibronectin was obtained from Collaborative Research Inc. Medium 199 was obtained from Gibco Inc. Fetal Bovine Serum was obtained from Hyclone Laboratories. Electric Cell Impedance Sensing (ECIS) microelectrodes were obtained from Applied Biophysics Inc. Cultured human umbilical vein endothelial cells (HUVEC) were obtained from the Tissue Culture Facility, College of Medicine at the University of Iowa.

3.2 Cell culturing and adhesion assay

Cultured human umbilical vein endothelial cells were prepared by the collagenase treatment of freshly obtained human umbilical veins. Harvested primary cultures designated for cell-adhesion assays were plated on 60-mm tissue culture plates that were coated with 100 μg/ml of fibronectin. All cells were cultured in Medium 199 supplemented with 20% heat-inactivated fetal calf serum, basal medium eagle vitamins and amino acids, glucose (5 mM), glutamine (2 mM), penicillin (100 U/ml), and streptomycin (100 μg/ml). Cultures were identified as endothelial cells by their characteristic uniform cobblestone morphology, uptake of acetylated low density lipoprotein, and by indirect immunofluorescent staining by factor VIII.

Cells were cultured on a small gold electrode, approximately $5 \cdot 10^4$ cells per unit cm^2 shown in Figure 4 using culture medium as the electrolyte, and barrier function was measured by determining the electrical impedance. The total impedance of the monolayer is composed of the impedance between the ventral surface of the cell and the electrode, the impedance between the cells and the impedance of two cell membrane in series.

3.3 Cell covered impedance $Z_c(\omega_i)$ and naked impedance $Z_n(\omega_i)$

Endothelial barrier function was measured in real time by measuring transendothelial impedance using material and cell culturing technique described above after cultures reached postconfluency about 24 hours or one-day-old. First, impedance measurements were obtained repeatedly at 23 different frequencies of 25Hz, 50Hz, 75Hz, 100Hz, 200Hz, 500Hz, 750Hz, 1kHz, 2kHz, 3kHz, 4kHz, 5kHz,

6kHz, 7kHz, 8kHz, 9kHz, 10kHz, 15kHz, 20KHz, 30kHz, 40kHz, 50kHz and 60kHz. The obtained data set is the measured cell covered impedance $Z_c(\omega_i)$, $i = 1, 2, , 23$, at those 23 frequencies. The measurement process took about 20 minutes. Then, cells were removed from the electrode with a solution of 0.5% trypsin and ethylenediaminetetraacetic acid. This removal process took approximately 15 minutes. Then, a repeat of impedance measurements was taken over the same 23 frequencies to obtain the naked cell impedance $Z_n(\omega_i)$, $i = 1, 2, , 23$. This measurement took about another 20 minutes.

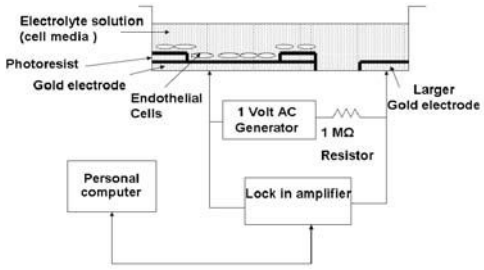

Fig. 5. Data collecting circuit illustration.

3.4 Data collection circuit

Data is collected for each experiment for a given frequency using the commercially available Electric Cell Impedance Sensing data acquisition system from Applied BioPhysics which can record 16 different tissue cultures (tissue wells) at a time. The data is collected for cells grown on a monopolar gold electrode array supplied with the Electric Cell Impedance Sensing data acquisition system that is comprised of a large counter electrode and a significantly small microelectrode on which the cellar monolayer is grown shown in Figure 4 and illustrated in Figure 5. The overall measurement system comprises of a microelectrode assembly as discussed above, a precision frequency detector (SRS830 lock-in amplifier, Stanford Instruments Inc.) to collect the impedance, a precision signal generator and a personal computer for data collection and subsequent data analysis. Under the control of computer, the reference signal generator is commanded to apply 1 volt AC signal of precise reference frequency through a 1-MΩ resistor to the microelectrode. The 1-MΩ resistor is included to provide the effect of having relatively constant current for all measurements at different frequencies taken during an experiment. The lock-in amplifier then measures the resultant in phase voltage and current components and out of phase voltage and current components across the microelectrode assembly, passing the measurement data back to the computer for storage and data analysis. The measurement process is repeated at 23 different frequencies for both cell-covered and naked microelectrodes.

3.5 Experiment results

A large number of experiments were carried on postconfluent cultured human umbilical vein endothelial cells. Experiments were conducted after culture reached postconfluency about one-day-old. Figure 6 is a typical result of the experiments with 14 wells (14 separate electrodes). Shown

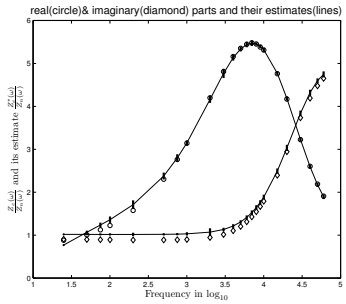

Fig. 6. The actual $\frac{Z_c(\omega)}{Z_n(\omega)}$ and its estimate.

in Figure 6 are the real and imaginary parts, respectively, of the predicted $Z_c^*(\omega_i)/Z_n(\omega_i)$ (solid) based on the model (2) with the estimates $(\alpha^*, R_b^*, R_m^*, c_m^*)$ derived from the Levenberg-Marquardt nonlinear least squares method [12] and the cost function (3), and the actually measured $Z_c(\omega_i)/Z_n(\omega_i)$ (circle=real part and diamond=imaginary part) at 23 different input frequencies. The bold vertical bars represent the standard deviations of the estimation errors between $Z_c(\omega_i)/Z_n(\omega_i)$ and $Z_c^*(\omega_i)/Z_n(\omega_i)$ at each frequency based on the measurements of 14 wells. In reality, no "true values" of α, R_b, c_m and R_m are available. One logical test is to see how the predicted $Z_c^*(\omega_i)/Z_n(\omega_i)$, based on the estimates α^*, R_b^*, R_m^* and c_m^*, fits the actually $Z_c(\omega_i)/Z_n(\omega_i)$ at input frequencies. Clearly, from Figure 6, a reasonable fit is obtained and this validates our approach and the model.

3.6 Discussion

It's important to emphasize that we are modeling endothelial cells, which do not display automaticity properties like muscle cells. There are no constitutive ion channel activity like epithelial cells or cardiac muscle. Also, we are examining the cell-membrane properties of a static resting cell and this does not mean that the model will predict a dynamic response under a more dynamic physiological change. Further, we make a few remarks.

- A number of experiments have been carried out and the results are consistent. All experiments are done on an one-day-old postconfluent monolayer of cultured endothelial cells. The timing is critical. If the measurements are made too early, the experimental results exhibit some random phenomenon because electrical properties during cell attachment are in the transition period and unreliable. The readings may become unreliable again if the measurements are made too late.
- The fit at the high frequency range is fairly good and there exists a relatively larger modeling error at low frequency range. Consistent low frequency errors are unlikely due to random noise but are a systematic under-modeling. There are several possibilities.
  (1) First, the impedance R_b between the adjacent edges of cells is modeled as a pure resistor. This could be overly simplified. Some marginal improvement at low frequencies may be achieved by modeling this impedance as a resistor and a capacitor in parallel.
  (2) The second reason is the nonlinearity and possibly time varying factors. In this paper, a cell sys-

tem is modeled by linear and constant resistors and capacitors in various connections. However, the actual cell system does exhibit some nonlinear and timing varying properties. The impedance changes with time. Moreover, changes at different frequencies are different, especially large changes at low frequency range. This implies the underlining cell system is not completely linear and time invariant that could be partially responsible for low frequency errors.

(3) The third reason is the assumption that the naked electrode impedance and the cell impedance are in series when the cells are grown on the electrode. Preliminary study seems to suggest that there is also a parallel structure when cells are grown on the electrode. The problem is that with additional parallel structure or nonlinearity, mathematical modeling becomes much more complicated. By exploiting their electrical paths and properties, the governing equation was derived in the paper which is a nonlinear partial differential equation involving time t and distance r. By examining only the steady state with a single frequency excitation, we were able to simplify the equation to a nonlinear ordinary equation. Fortunately, analytic solution exists that leads to the model derived in the paper. With additional parallel structure or nonlinearity, the resultant nonlinear equation does not seem to be representable in a clean way let alone analytic solution. This is the topic that we are working on.

4. CONCLUDING REMARKS

Though there exist some low frequency errors and steps discussed above can be employed to improve the model, the fits are generally good. This suggests that the numerical model and algorithms presented in the paper can be utilized for several essential applications for cell biologists and cell physiologists; (1) The model can be applied to evaluate how exogenous physiological and pathological stimuli regulate endothelial barrier function. (2) The model can be applied to quantify and elucidate with precision cell-cell interactions between leukocyte-endothelial and pathogen-host interactions. (3) The model is useful to elucidate signal transduction pathways that regulate cell membrane properties under different experimental conditions. (4) The model has utility to precisely evaluate how genomics and proteonomics of the cytoskeleton regulate cell membrane properties in intact living cells in which the behavior of the cytoskeleton may not be adequately predicted from *in vitro* bioinformatics tools. (5) The numerical model can be used to evaluate molecular mechanism of drug toxicity. The numerical model could be multiplexed with electrical and optical based assays to evaluate molecular mechanisms of drug therapeutics and toxicity.

REFERENCES

[1] Bodmer J, A. English, M. Brady, K. Blackwell, K. Haxhinasto, S. Fotedar, K. Borgman, E.W. Bai, and A. Moy. (2005), "Modeling Error and Stability of Endothelial Cytoskeletal-Membrane Parameters Based on Modeling Transendothelial Impedance as Resistor and Capacitor in series, *AJP-Cell, Physiology*, **289**:C735-C747

[2] Chand, M., S. Shaby and D. Shaby (1989), "Histamine and ionositol phosphate accumulation in endothelium cAMP and G-protein", *Am J. Physiolo*, **257**:L259-L264.

[3] Giaever I and Keese CR. (1984), "Monitoring fibroblast behavior in tissue culture with an applied electric field", *Proc Natl Acad Sci*, **81**:3761-3764

[4] Giaever I and Keese CR. (1986), "Use of electric fields to monitor the dynamical aspect of cell behavior in tissue culture", *IEEE Transactions on Biomedical Engineering*, **33**: 242-247

[5] Haxhinasto, K., A. Kamath, K. Blackwell, J. Bodmer, A.English, E.W. Bai and A. Moy (2004), "l-Caldmon alters cytoskeletal-membrane function independent of myosin AToase and actin assembly in fibroblasts", *Am J. Physiol Cell Physiology*, **287**:C1125-C1138

[6] Kimura, K., M. Ito, M. Amano, C. Fukata, K. Nakafuku, A. Iwamatsu, and K. Kaibuchi (1996), "Regulation of myosin phatase by Rho and Rho-associated kinase", *Science*, **273**:245-248.

[7] Ljung L. (1987), System Identification: Theory for the user, Prentice-Hall

[8] Moy A, Blackwell K, and A. Kamath A (2002), "Differential effects of histamine and thrombin on endothelial barrier function through actin-myosin tension", *Am Journal of Physiol - Heart and Circulatory Physiology* **282**:H21-H29

[9] Moy AB, VanEngelenhoven J, Bodmer J, Kamath J, Keese C, Giaever I, Shasby S, and Shasby DM (1996) "Histamine and Thrombin Modulates Endothelial Focal Adhesion Through Centripetal and Centrifugal Forces", *J Clin Invest*, **97**:1020-1027.

[10] Moy AB, Winter M, Kamath A, Blackwell K, Reyes G, Giaever I, Keese C, and Shasby DM (2000), "Histamine alters endothelial barrier function at cell-cell and cell-matrix sites", *American Journal of Physiology - Lung Cellular & Molecular Physiology*, **278**:L888-898.

[11] Pintelon R. and J. Schoukens (2001), System Identification: A Frequency Domain Approach, Wiley

[12] Press, W., B. Flannery, S. Teukolsky and W. Vetterling (1992), NUMERICAL RECEIPES IN C, 2nd Ed. Cambridge University Press, Cambridge, UK

[13] Schneeberger, E. and R. Lynch (1984), "Tight junctions, composition and function", *Circ Res*, **55**:723-733.

[14] Silvia, N., L. Mazzetti, P. Failli and D. Bani (2002), "High yield method for isolation and culture of endothelial cells from rat coronary blood vessels suitable for analysis of interacellular calcium and nitric oxide biosynthetic pathway", *Bio. Proced. On-line*, **4**:32-37.

[15] Soderstrom T and P Stoica (1989), System Identification, Prentice-Hall

[16] Tiruppathe, C., A. Malik, P. Vecchio, C. Keese and I. Giaever (1992), "Electrical method for detection of endothelial cell shape change in real time assessment of endothelial barrier function", *Proc. Natl. Acad. Sci*, **89**:7919-7923.